

Do unequal-mass binary black hole systems have larger χ_{eff} ? Probing correlations with copulas in gravitational-wave astronomy

Christian Adamcewicz^{1,2*} and Eric Thrane^{1,2}

¹*School of Physics and Astronomy, Monash University, Clayton VIC 3800, Australia*

²*OzGrav: The ARC Centre of Excellence for Gravitational Wave Discovery, Clayton VIC 3800, Australia*

Accepted XXX. Received YYY; in original form ZZZ

ABSTRACT

The formation history of binary black hole systems is imprinted on the distribution of their masses, spins, and eccentricity. While much has been learned studying these parameters *in turn*, recent studies have explored the *joint* distribution of binary black hole parameters in two or more dimensions. Most notably, it has recently been argued that binary black hole mass ratio and effective inspiral spin χ_{eff} are anti-correlated. We point out a previously overlooked subtlety in such two-dimensional population studies: in order to conduct a controlled test for correlation, one ought to fix the two marginal distributions—lest the purported correlation be driven by improved fit in just one dimension. We address this subtlety using a tool from applied statistics: the copula density function. We use the previous work correlating mass ratio and χ_{eff} as a case study to demonstrate the power of copulas in gravitational-wave astronomy while scrutinising their astrophysical inferences. Our findings, however, affirm their conclusions that binary black holes with unequal component masses exhibit larger χ_{eff} (98.7% credibility). We conclude by discussing potential astrophysical implications of these findings as well as prospects for future studies using copulas.

Key words: gravitational waves – stars: black holes – binaries: general – transients: black hole mergers

1 INTRODUCTION

There is still much uncertainty surrounding the astrophysics of binary black hole (BBH) formation (see the reviews by [Mapelli 2018](#); [Mandel & Farmer 2022](#); [Spera et al. 2022](#), for example). Nonetheless, some general features can be associated with different formation channels. Binaries assembled in the field are likely to contain black holes with spin vectors that are preferentially aligned to the orbital angular momentum vector ([Mandel & de Mink 2016](#); [Belczynski et al. 2016a](#); [Stevenson et al. 2017](#); [Marchant et al. 2016](#); [Talbot & Thrane 2017](#); [Qin et al. 2018](#)). The vast majority of these systems should be nearly circular (negligible eccentricity) ([Peters 1964](#); [Hinder et al. 2008](#)) and they ought to include black holes with masses below the pair instability gap ([Belczynski et al. 2016b](#); [Marchant et al. 2019](#); [Stevenson et al. 2019](#); [Woosley & Heger 2021](#)). Binaries assembled dynamically in dense stellar environments are likely to contain black holes with isotropic random spin orientations ([Schnittman 2004](#); [Bogdanović et al. 2007](#); [Rodríguez et al. 2015, 2016](#); [Stone et al. 2016](#); [Yu et al. 2020](#)). Some fraction of these systems, perhaps $\approx 5\%$, may be measurably eccentric ([Samsing et al. 2014](#); [Samsing & Ramirez-Ruiz 2017](#); [Samsing 2018](#); [Lower et al. 2018](#); [Zevin et al. 2019](#); [Romero-Shaw et al. 2019](#); [Gondán & Kocsis 2021](#)). These binaries may include ‘second-generation’ black holes in the pair instability mass gap ([O’Leary et al. 2016](#); [Fishbach et al. 2017](#); [Gerosa & Berti 2017](#); [Rodríguez et al. 2018](#); [Kimball et al. 2020, 2021](#); [Doctor et al. 2020](#)). By fitting the observed distribution of BBH masses, spins, and eccentricity, it is possible to estimate the fraction of BBH systems assembled through each of these channels (see [Abbott et al.](#)

[2019, 2021d,a](#); [Wong et al. 2021](#); [Farr et al. 2018](#); [Baibhav et al. 2020](#); [Zevin et al. 2021](#); [Bouffanais et al. 2021](#); [Roulet et al. 2021](#), and references therein).

To date, the majority of population modelling in gravitational-wave astronomy has been carried out using models where parameters factorise into statistically independent distributions. This was a reasonable starting point, providing a simple framework for the analysis of a relatively small dataset. However, as the number of gravitational-wave detections has increased, there has been growing interest in multivariate models, which allow for two or more parameters to be correlated; namely effective inspiral spin χ_{eff} with mass ([Safarzadeh et al. 2020](#); [Hoy et al. 2022](#); [Biscoveanu et al. 2022](#); [Franciolini & Pani 2022](#); [Tiwari 2022](#)), χ_{eff} with mass ratio ([Callister et al. 2021](#); [Franciolini & Pani 2022](#); [Tiwari 2022](#)), χ_{eff} with redshift ([Biscoveanu et al. 2022](#); [Bavera et al. 2022](#); [Tiwari 2022](#)), and redshift with mass ([Fishbach et al. 2021](#); [Belczynski et al. 2022](#)). This shift is motivated by theoretical studies, predicting multivariate distributions in χ_{eff} and mass (as well as mass ratio) ([Bavera et al. 2021, 2022](#); [Broekgaarden et al. 2022](#)), χ_{eff} and redshift ([Bavera et al. 2020](#)), redshift and mass ([Neijssel et al. 2019](#); [van Son et al. 2022](#); [Mapelli et al. 2022](#)), as well as mass ratio and component spin ([Lousto et al. 2010](#)). In [Kruckow & Han \(2021\)](#), the authors also propose that there is a correlation between the total mass and chirp mass. However, such a correlation would seem hard to avoid barring a pathological relationship between mass ratio and total mass.

We highlight one notable study, being [Callister et al. \(2021\)](#), which finds evidence for an anti-correlation between mass ratio and χ_{eff} . This was somewhat surprising, as theoretical studies prior to this work had only predicted such a multivariate distribution in the case of two rather specific BBH formation channels. The first of these is

* E-mail: cada0007@student.monash.edu

formation via common envelope evolution in binaries with very high common envelope efficiency, whilst the second is via stable mass transfer when supposing super-Eddington accretion (Bavera et al. 2021; Zevin & Bavera 2022). Follow-up studies suggested that this anti-correlation may also occur in BBH systems that undergo mass ratio reversal during stable mass transfer (Broekgaarden et al. 2022), as well as in BBH systems assembled dynamically in active galactic nuclei (AGN) (McKernan et al. 2022). If it is real, this covariance is an important clue for our understanding of BBH formation.

In this paper, we point out an important subtlety associated with multivariate population models. We are particularly concerned with studies that seek to establish a correlation κ between two parameters (x, y) . The details are somewhat technical (see Section 2), but the basic idea is that models in previous studies are constructed so that our assumptions about the distribution of y depend on the correlation parameter κ . This is not ideal because it means two knobs are always being changed at the same time: the degree of correlation and the shape of the y distribution. As a consequence, if one value of κ is preferred over another, it is not clear if this is due to a bona fide correlation or due to an improved fit to the shape of the y distribution. We show how this problem is solved using a tool from applied statistics: copulas (detailed in Sklar 1996).

Copulas have seen extensive application modelling covariance, especially in finance (see Bouyé et al. 2000, for an overview). Here, we present a few examples of copula applications in astronomy. First, copulas have been used to model covariance between bands in luminosity functions (Takeuchi 2010; Takeuchi et al. 2013; Andreani et al. 2014; Yuan et al. 2018), model multivariate mass functions (Takeuchi & Kono 2020), and model mass-luminosity correlations (Gunawardhana et al. 2014; Andreani et al. 2018) in galaxies. Copulas have also been used in cosmology—estimating cosmological parameters from gravitational lensing surveys (Sato et al. 2010; Lin & Kilbinger 2015), and modelling the dark matter density field (Scherrer et al. 2009; Qin et al. 2020). As a final example, copula models have been used to look for period-mass relations in extrasolar planetary systems (Jiang et al. 2008).

The remainder of this paper is organized as follows. In Section 2, we investigate the challenges of two-dimensional models, using Callister et al. (2021) as a case study. In Section 3, we show how these challenges are addressed with copulas. In Section 4, we use this framework to propose a new model for the distribution of BBH mass ratio and effective inspiral spin. We present our results in Section 5. We conclude in Section 6 and discuss how this work may be extended in the future.

2 THE CHALLENGES OF TWO-DIMENSIONAL MODELS

We are interested in the class of problems where one seeks to establish if there is a correlation present in two parameters (x, y) . As a case study, we dissect the model from Callister et al. (2021), which is focused on the parameters of mass ratio

$$q \equiv \frac{m_2}{m_1}, \quad (1)$$

and effective inspiral spin (Damour 2001)

$$\chi_{\text{eff}} = \frac{\chi_1 \cos t_1 + q \chi_2 \cos t_2}{1 + q}, \quad (2)$$

though, the problem is a quite general one. Here, m_1 and m_2 are the primary and secondary component masses of the binary. The mass ratio is allowed to vary on the interval $[m_{\text{min}}/m_1, 1]$. Meanwhile, χ_1 and χ_2 are the corresponding dimensionless spin magnitudes, and

t_1 and t_2 are the tilt angles between each spin vector and the orbital angular momentum.

The first step in Callister et al. (2021) (and similar gravitational-wave studies; Safarzadeh et al. 2020; Biscoveanu et al. 2022) is to make some assumption about the distribution of one parameter, in this case, mass ratio. Callister et al. (2021) adopt a power-law distribution

$$\pi(q|m_1, \Lambda) \propto q^\gamma. \quad (3)$$

Here, γ is one of the several hyper-parameters describing the BBH population—the set of which we denote Λ . Specifically, γ controls the shape of the marginal distribution for mass ratio. As the distribution of mass ratio is subtly conditioned on primary mass, it is worth noting that the primary mass distribution follows the power-law and peak model proposed by Talbot & Thrane (2018), such that

$$\pi(m_1|\Lambda) = f_p \mathcal{P}(m_1|\Lambda) + (1 - f_p) \mathcal{N}(m_1|\Lambda). \quad (4)$$

Here,

$$\mathcal{P}(m_1|\Lambda) \propto m_1^\lambda, \quad (5)$$

is a power-law,

$$\mathcal{N}(m_1|\Lambda) \propto \exp \left[-\frac{(m_1 - \mu_m)^2}{2\sigma_m^2} \right], \quad (6)$$

is a Gaussian feature, and f_p is a hyper-parameter that denotes the fraction of BH masses in the power-law component. Of course, λ , μ_m , and σ_m are also hyper-parameters.

The next step is to assume some functional form for the distribution of the second variable *conditioned on the first variable*. Callister et al. (2021) assume

$$\pi(\chi_{\text{eff}}|q, \Lambda) \propto \exp \left[-\frac{(\chi_{\text{eff}} - \mu_\chi(q, \Lambda))^2}{2\sigma_\chi(q, \Lambda)^2} \right]. \quad (7)$$

This is a Gaussian distribution with a mean that depends on the mass ratio:

$$\mu_\chi(q, \Lambda) \equiv \mu_{\chi,0} + \alpha(q - 0.5). \quad (8)$$

Here, $\mu_{\chi,0}$ and α are two more hyper-parameters. The α parameter controls the degree of covariance; the covariance vanishes when $\alpha = 0$. The width of the Gaussian is also conditioned on mass ratio:

$$\log_{10} \sigma_\chi(q, \Lambda) \equiv \log_{10} \sigma_{\chi,0} + \beta(q - 0.5). \quad (9)$$

Here, $\sigma_{\chi,0}$ and β are also hyper-parameters.

The model is fit to LIGO–Virgo (Aasi et al. 2015; Acernese et al. 2015) data, using GWTC-2 (Abbott et al. 2021b,c) in order to obtain posterior distributions for the hyper-parameters describing the distribution of BBH mass and spin. Callister et al. (2021) finds support for a negative value of $\alpha = -0.46^{+0.29}_{-0.28}$ (90% credibility). These results seem to imply a significant anti-correlation between mass ratio and effective inspiral spin, as seen in the left panel of Fig. 1. In fact, a value of $\alpha \geq 0$ is ruled out by Callister et al. (2021) with a credibility of 98.7%.

However, given the way this model is constructed, different hyper-parameter values for α or β produce different marginal distributions for χ_{eff} :

$$\pi(\chi_{\text{eff}}|\Lambda) = \int_{q_{\text{min}}}^1 dq \pi(\chi_{\text{eff}}|q, \Lambda) \pi(q|\Lambda). \quad (10)$$

This is dramatically illustrated in Fig. 1, which shows two different marginal distributions $\pi(\chi_{\text{eff}}|\Lambda)$ —one with an $\alpha < 0$ anti-correlation

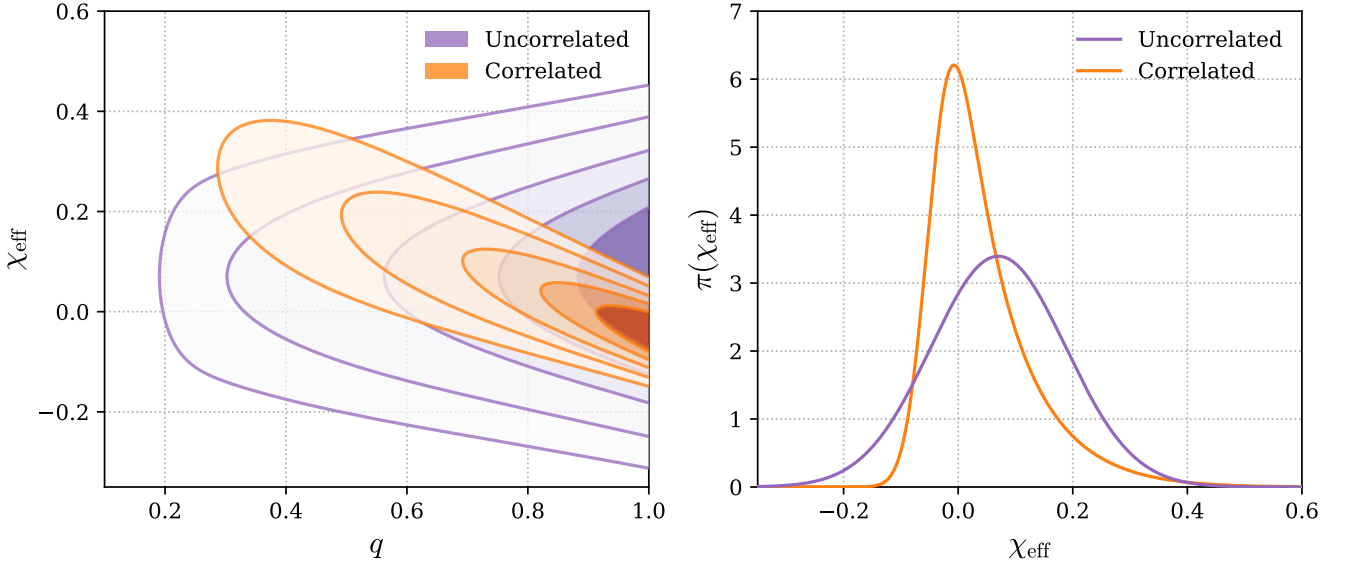


Figure 1. Reconstructed distributions using the best-fit parameters from Callister *et al.* (2021). In purple is the uncorrelated model, whilst the correlated model is shown in orange. **Left:** the joint distributions for mass ratio and effective inspiral spin. **Right:** the marginal distributions for effective inspiral spin. Note how the act of marginalisation produces a highly skewed, non-Gaussian distribution for the orange correlated model.

(orange) and one with no correlation (purple). Introducing covariance between (q, χ_{eff}) has reshaped the marginal distribution of χ_{eff} . This begs the question: *why* do the data prefer $\alpha < 0$ —is it because there is truly a correlation between (q, χ_{eff}) ; or is it because the χ_{eff} distribution in nature is better described as asymmetric (orange) than symmetric (purple); or is it some combination of both factors?

While this is a potential issue with all correlation studies that utilise this framework, the case of q and χ_{eff} is particularly interesting. As noted in Callister *et al.* (2021), their asymmetric fit for $\pi(\chi_{\text{eff}}|\Lambda)$ (see Fig. 1) is qualitatively similar to the results of Roulet *et al.* (2021). Furthermore, Galaudage *et al.* (2021) finds a significant zero-spin peak in the distribution of BBH spin magnitudes (χ_1 and χ_2), although follow-up studies in Callister *et al.* (2022) and Mould *et al.* (2022) find no such feature. Regardless, this may raise the question of whether the orange correlated marginal distribution in Fig. 1 is favourable, due to increased support near $\chi_{\text{eff}} = 0$, when compared to the purple uncorrelated case. We therefore seek to determine if the correlation observed by Callister *et al.* (2021) can be explained away as an artifact of their model construction.

3 COPULAS

In order to address the challenges identified in the previous section, we seek to construct a model in which covariance can be introduced without changing the marginal distributions for either (q, χ_{eff}) . Copulas are a tool from applied statistics for exactly this purpose (Sklar 1996). In this section, we provide an introduction to copulas. This will provide the foundation upon which we will build our new model for (q, χ_{eff}) in Section 4. Whilst copulas traditionally refer to cumulative distribution functions (see Sklar 1996), we use the term as a short-hand for their related copula density functions. Formally, a copula density function is any joint probability distribution $\pi_c(u, v|\kappa)$, for parameters $u, v \in [0, 1]$, with *uniform* marginal distributions for

both u and v

$$\pi(u|\kappa) = \int_0^1 dv \pi_c(u, v|\kappa) = 1 \quad (11)$$

$$\pi(v|\kappa) = \int_0^1 du \pi_c(u, v|\kappa) = 1, \quad (12)$$

conditioned on hyper-parameter κ , which controls the degree of correlation between (u, v) . Applied statisticians have derived a large variety of copulas, each providing a unique shape for the joint distribution when $\kappa \neq 0$. Different shapes are suitable for different physical models. Examples of different copulas are shown in Fig. 2.

In general, physical parameters are not distributed uniformly on the interval $[0, 1]$. However, physical parameters (x, y) are easily related to copula parameters (u, v) using cumulative density functions:

$$u(x) = \int_{x_{\min}}^x dx' \pi(x') \quad (13)$$

$$v(y) = \int_{y_{\min}}^y dy' \pi(y'). \quad (14)$$

Thus, we may construct a distribution for (x, y) as

$$\pi_c(x, y|\kappa) = \pi(x)\pi(y)\pi_c(u(x), v(y)|\kappa), \quad (15)$$

which preserves the (non-uniform) marginal distributions for x and y , while allowing the covariance to change according to κ . Technically, $\pi_c(x, y|\kappa)$ is not a copula because x and y are not uniformly distributed, but as shorthand, we refer to this distribution as a copula for (x, y) .

4 MODEL AND IMPLEMENTATION

In this section, we construct a copula model for $\pi(q, \chi_{\text{eff}})$. The first step is to choose marginal distributions for $\pi(q)$ and $\pi(\chi_{\text{eff}})$, which we choose to match the correlated model from Callister *et al.* (2021). The distribution of mass ratio is therefore taken to be a

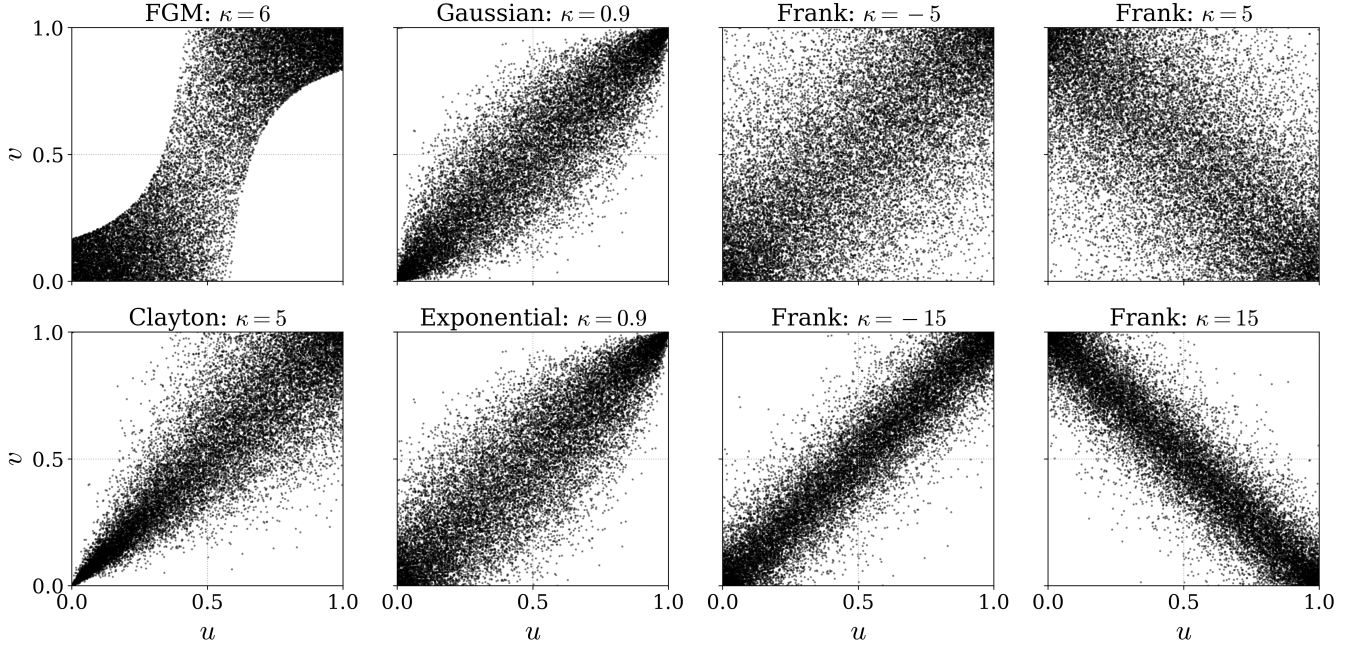


Figure 2. Examples of copula density functions. The different values of κ yield different degrees of correlation. Note in every case, the marginal distributions for u and v are uniformly distributed. When $\kappa = 0$, there is no correlation present, which would correspond to a two-dimensional uniform distribution (a featureless square). As κ increases in magnitude, a correlation or an anti-correlation is introduced, depending on the sign of κ and the type of copula density function used. Listed above each example is the name of the copula density function and the value of κ used.

Parameter	Prior	Description
$\mu_{\chi,0}$	$\mathcal{U}(-1, 1)$	Mean of Gaussian χ_{eff} distribution when $\alpha = 0$
$\log_{10} \sigma_{\chi,0}$	$\mathcal{U}(-1.5, 0.5)$	Log standard deviation of Gaussian χ_{eff} distribution when $\beta = 0$
α	$\mathcal{U}(-2.5, 1)$	Reshapes the χ_{eff} distribution through q
β	$\mathcal{U}(-2, 1.5)$	Reshapes the χ_{eff} distribution through q
μ_m	$\mathcal{U}(20M_{\odot}, 100M_{\odot})$	Mean of Gaussian peak in m_1 distribution
σ_m	$\mathcal{U}(1M_{\odot}, 10M_{\odot})$	Standard deviation of Gaussian peak in m_1 distribution
f_p	$\mathcal{U}(0, 1)$	Fraction of m_1 in the Gaussian peak
λ	$\mathcal{U}(-5, 4)$	Index for power-law component of m_1 distribution
γ	$\mathcal{U}(-2, 10)$	Index for power-law distribution of q
m_{max}	$\mathcal{U}(60M_{\odot}, 100M_{\odot})$	Maximum possible BH mass
m_{min}	$\mathcal{U}(2M_{\odot}, 10M_{\odot})$	Minimum possible BH mass
κ	$\mathcal{U}(-100, 100)$	Determines the level of correlation between q and χ_{eff}

Table 1. List of hyper-parameters used in the model defined in Section 4 along with their respective priors. Here, $\mathcal{U}(a, b)$ indicates a uniform distribution on the interval $[a, b]$.

power-law; see equation 3. There is some complication because the distribution of q is subtly conditioned on primary mass m_1 —since we require each component mass to be on the interval $(m_{\text{min}}, m_{\text{max}})$, not all values of q are allowed for some values of m_1 . We there-

fore marginalize numerically over m_1 ¹. The distribution of χ_{eff} is obtained numerically by marginalizing over q in equation 7; see the right-hand panel of Fig. 1. Using the marginal distributions of

¹ Primary mass is distributed according to a power-law and Gaussian peak mixture model such that $\pi(m_1 | \Lambda)$ follows equation 4.

(q, χ_{eff}) , we compute the copula variables (u, v) following Eqs. 13–14.

The next step is to choose a copula. We opt to use the Frank copula density function:

$$\pi_c(u, v|\kappa) = \frac{\kappa e^{\kappa(u+v)}(e^\kappa - 1)}{(e^\kappa - e^{\kappa u} - e^{\kappa v} + e^{\kappa(u+v)})^2}, \quad (16)$$

which we chose by trial and error on the grounds that it produces physically plausible-looking correlations (to our eyes) in the (q, χ_{eff}) plane; see the right four panels of Fig. 2. The subjectivity associated with the choice of copula is similar to other model-building choices, e.g., the functional form of $\pi(\chi_{\text{eff}}|q)$. However, in principle, one may perform model selection to choose between copulas. Finally, we use equation 15 to define $\pi_c(q, \chi_{\text{eff}}|\Lambda, \kappa)$.

By construction, our model is similar to the model from Callister et al. (2021). The two models share hyper-parameters, though, our model has an additional parameter κ . There is, however, an important difference. In Callister et al. (2021), the α parameter controls the correlation between (q, χ_{eff}) —while also inadvertently changing the marginal distribution for χ_{eff} . However, in our model, α is used only to change the marginal distribution for χ_{eff} . The same can be said of β . The covariance between (q, χ_{eff}) is determined entirely with κ .

With our model now defined, the next step is to carry out population inference to obtain posterior distributions for the hyper-parameters—especially κ . With each sampling step, the copula variables (u, v) are reevaluated to reflect the newly proposed values Λ , and the corresponding marginal distributions $\pi(q|\Lambda)$ and $\pi(\chi_{\text{eff}}|\Lambda)$. We employ the population inference package GWPoPulation (Talbot et al. 2019), which employs Bilby (Ashton et al. 2019; Romero-Shaw et al. 2020). We use the nested sampler DYNesty (Speagle 2020). We use the same 44 BBH events from GWTC-2 (Abbott et al. 2021b,c) as Callister et al. (2021). In reweighting this data, we utilise the fiducial prior for χ_{eff} derived in Callister (2021). The priors for Λ are listed in Table 1.

5 RESULTS

In Fig. 3, we show in blue the reconstructed marginal distributions of q and χ_{eff} , as well as the associated joint distribution obtained from our fit. Overlaid in orange is the maximum-posterior fit from Callister et al. (2021). As expected, the marginal distribution of mass ratio is effectively identical in either case. We recover a similar marginal distribution for χ_{eff} when modelling its shape separately from the correlation. In hindsight, this is perhaps unsurprising given the preference for this asymmetric shape seen in previous work (Roulet et al. 2021; Galaudage et al. 2021). Turning our attention to the joint distribution, we find support for an anti-correlation between mass ratio and effective inspiral spin similar to the one inferred by Callister et al. (2021). This indicates that the anti-correlation described by Callister et al. (2021) is unlikely to be just a byproduct of the marginal distribution $\pi(\chi_{\text{eff}})$ ². In Fig. 4, we show the same reconstruction for the copula model, this time using the mean constructed via 500 hyper-parameter draws from their associated posteriors.

Whilst the anti-correlation hypothesis is well supported, we cannot

entirely rule out the possibility of no correlation at high credibility. Indeed, examining the posterior distribution for κ in Fig. 5, we find that $\kappa = 0$ is ruled out with 98.7% credibility, the same significance obtained in Callister et al. (2021)³. Meanwhile, we obtain credible intervals of $\alpha = -0.53^{+0.76}_{-0.44}$ and $\beta = -1.03^{+1.56}_{-0.86}$, which are similar to the values found in Callister et al. (2021): $\alpha = -0.46^{+0.29}_{-0.28}$ and $\beta = -0.83^{+1.28}_{-1.01}$. This is in spite of the fact that, in our model, α and β have no effect on the (q, χ_{eff}) covariance—they only affect the shape of the χ_{eff} distribution.

6 DISCUSSION

We find some evidence in support of the idea that mass ratio and effective inspiral spin are anti-correlated, corroborating the findings of Callister et al. (2021). Our results demonstrate that the significance of Callister et al. (2021)’s anti-correlation is not arising entirely from an improvement in the χ_{eff} fit. This has potential implications for the formation channels of BBH systems observed in gravitational waves. Several of these are already discussed in Callister et al. (2021), but we discuss them here for completeness.

First, simulations by Broekgaarden et al. (2022) suggest that BBH systems, which undergo mass ratio reversal (where the second born BH accretes enough mass to become the heavier BH in the binary) may exhibit anti-correlation in the $q - \chi_{\text{eff}}$ plane. Similar anti-correlation is predicted by Bavera et al. (2021) when assuming BBH systems are formed through either common envelope evolution with high common envelope efficiency, or through stable mass transfer using super-Eddington accretion. The preference for a qualitatively similar anti-correlation seen here may indicate that a large portion of BBH merger events observed to date come from one or more of the three aforementioned scenarios.

Another potential explanation for this feature, proposed by Callister et al. (2021), is that the anti-correlation is produced via the Simpson’s paradox (see Blyth 1972). According to this hypothesis, the population of BBH merger events does not exhibit anti-correlation locally, but it appears globally due to groupings of separate sub-populations in the $q - \chi_{\text{eff}}$ plane, potentially born through a mixture of different formation channels. Through model selection, it may be possible to distinguish between these two scenarios.

In a follow up to Callister et al. (2021), McKernan et al. (2022) suggest that a (q, χ_{eff}) anti-correlation may arise from BBH systems forming dynamically in AGN, provided several assumptions hold: black holes in the AGN disk are heavier and have aligned spins whilst those outside are lighter and have random spin alignments; the inner AGN disk is dense but small; and migration of black holes into the disk is turbulent. If one could show this phenomenological anti-correlation aligns with these predictions, the above properties may apply to AGN more generally (Vajpeyi et al. 2022).

Given that the definition of χ_{eff} is dependent on q (see equation 2), one might expect some degree of covariance in (q, χ_{eff}) is implied even if component spin parameters are distributed independently. We investigate this in Appendix Section A, finding that the

² The joint distribution implied by the copula model also exhibits a subtle widening as q approaches unity. As can be seen in Fig. 2, copulas tend to exhibit regions of relatively high density in the corners in order to keep the marginal distributions of u and v flat near 0 and 1. This can lead to kinks in joint distributions constructed with copula density functions, such as the one seen here.

³ Note that the support for $\kappa = 100$ (the upper bound of the prior) is non-zero. This raises the question of whether it is necessary to extend the bounds of the prior on κ . However, the correlation does not change much beyond values of $\kappa = 100$, which is already an extremely tight anti-correlation. Extending the prior boundary results in a long, low-density tail. This yields a subtle $\sim 0.1\%$ increase in the credibility for anti-correlation.

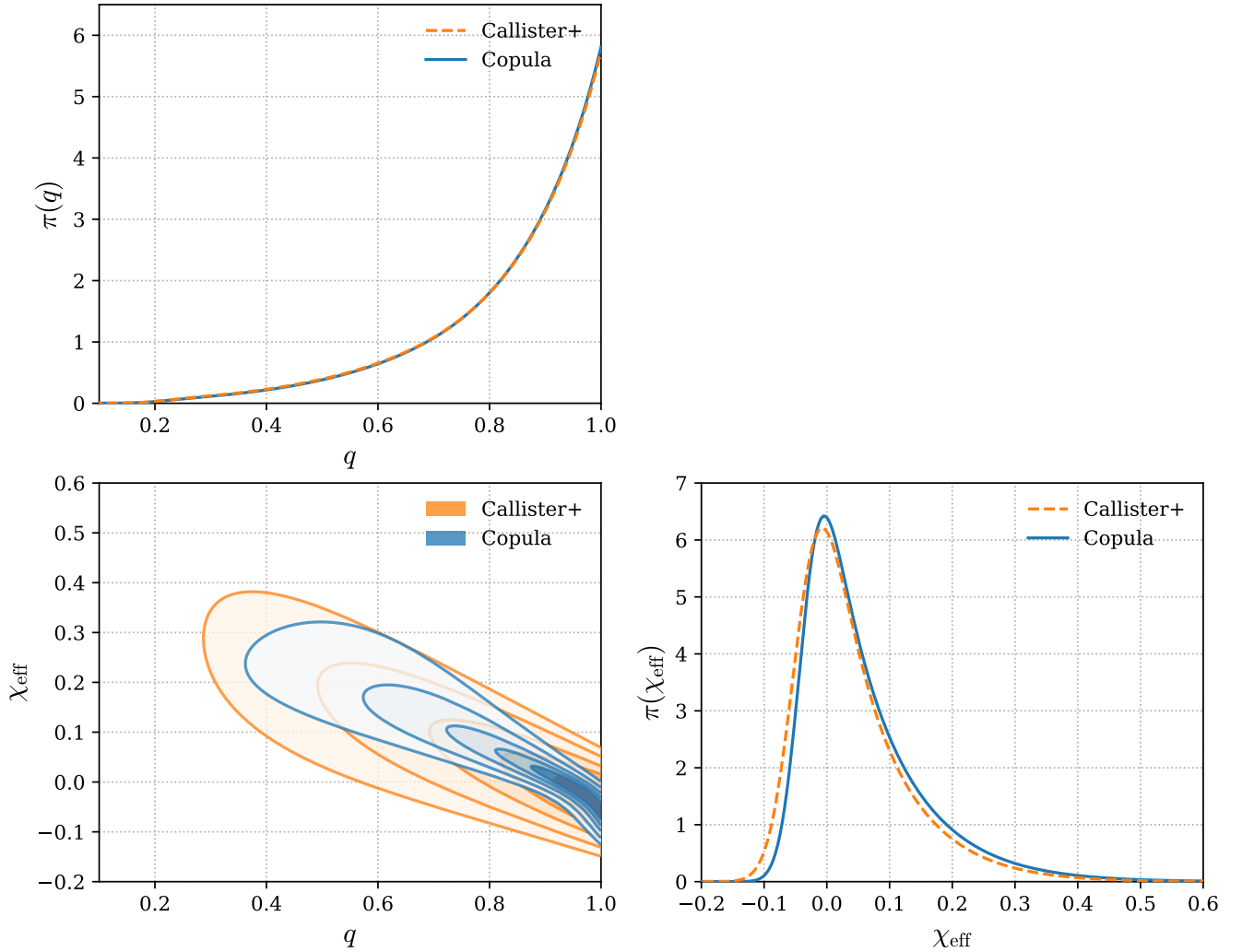


Figure 3. Reconstructed distributions for the Callister *et al.* (2021) model (orange) and the copula model from Section 4 (blue) using maximum posterior values for all hyper-parameters. **Top left:** the marginal distributions of mass ratio. **Bottom right:** the marginal distributions of effective inspiral spin. **Bottom left:** the joint distributions for mass ratio and effective inspiral spin.

level of correlation exhibited in our results cannot be implied by the parameterisation of χ_{eff} alone.

We now turn our attention from the astrophysical implications of our results to the use of copulas in gravitational-wave astronomy. There are many different existing copula density functions. This provides the potential to probe not only the level of correlation between two parameters x and y , but also the precise shape of the correlation in the $x - y$ plane. Model comparisons for marginal distributions such as those in Abbott *et al.* (2019) (see also the tutorial by Thrane & Talbot 2019) can be simply adapted to compare the fit of several different copula density functions. This can be used to look for subtle features in the covariance.

It is natural to ask if the principles described in this paper can be extended to look for correlations in > 2 dimensions. Progress has been made creating three-dimensional copulas (e.g. Sklar 1996; Bedford & Cooke 2002; Aas *et al.* 2009; Devroye & Letac 2010), although the vast majority of literature on this topic involves correlations in just two dimensions. Nevertheless, it is possible to identify complicated correlations in large-dimension spaces using a formalism like

this. One method for doing so is through use of ‘vine copulas’ (Bedford & Cooke 2002). This framework effectively stitches together multiple two-dimensional copulas, allowing for an infinitely scalable n -dimensional copula (see Takeuchi & Kono 2020, for an example applied to galactic mass-luminosity functions).

We see copulas as essential for model testing, but not necessarily for model building. The ‘dependent-distribution’ models used in Callister *et al.* (2021), Safarzadeh *et al.* (2020), and Biscoveanu *et al.* (2022) are all, in our view, physically reasonable. However, having identified that a correlation might be present with such a dependent-distribution model, follow-up study with a copula is indispensable in order to determine if the correlation is bona fide, or due to a improvement in the dependent-parameter marginal distribution.

Given the large number of questions and competing theories for BBH formation, the study of covariance between astrophysical parameters is likely to be useful for future investigations. Copulas are effective tools for measuring covariance in gravitational-wave astronomy. They allow us to eliminate extraneous and potentially confounding changes to models when testing for correlation, with results that

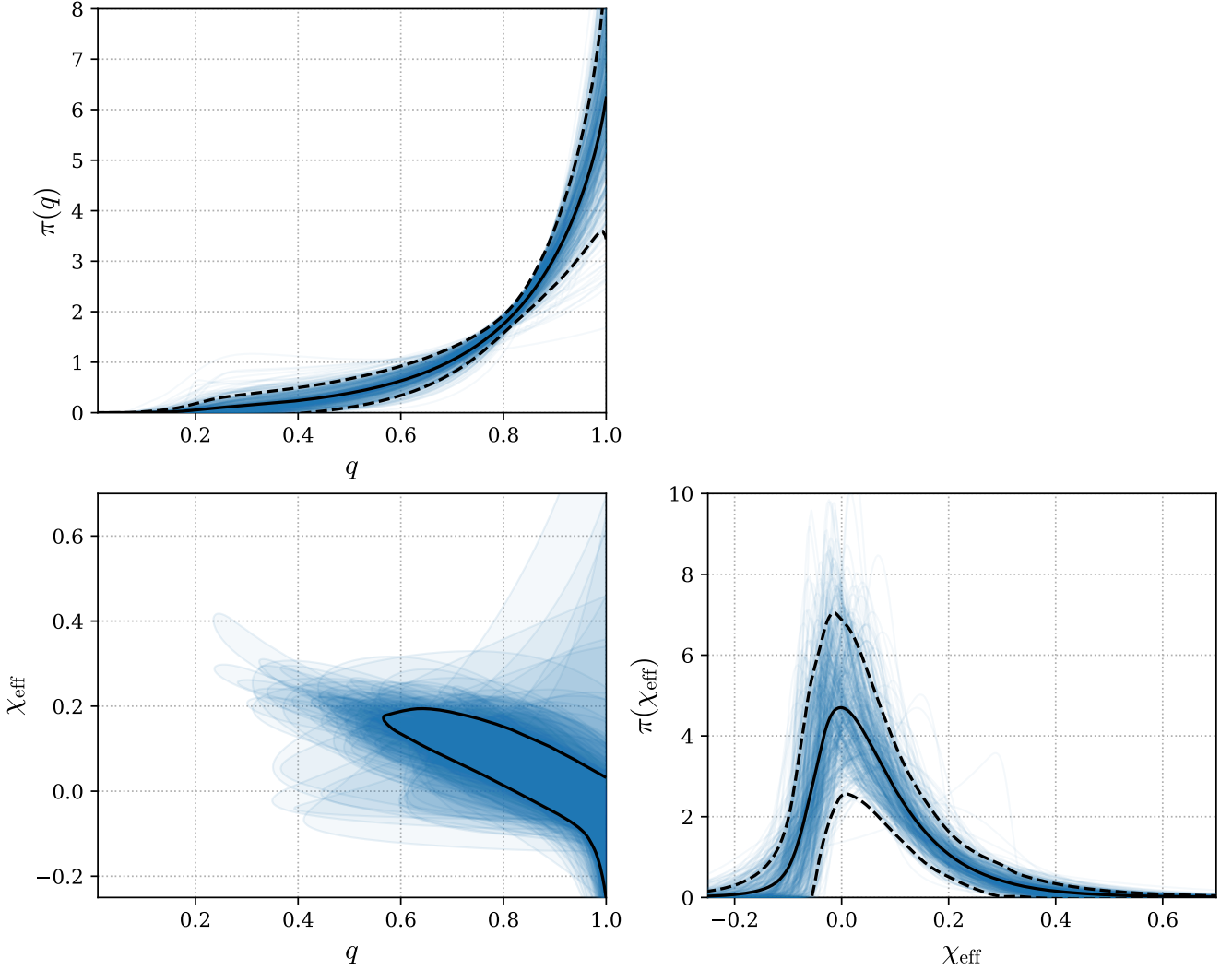


Figure 4. Posterior predictive distributions for the copula model presented in Section 4. **Top left:** the marginal distribution of mass ratio. **Bottom right:** the marginal distribution of effective inspiral spin. **Bottom left:** the joint distribution for mass ratio and effective inspiral spin. In the one-dimensional plots, the blue lines trace distributions implied by 500 random draws from the posteriors of the hyper-parameters. The solid black lines shows the mean distribution, whilst the dashed lines encapsulate the 90%-credible regions. In the two-dimensional plot, the blue segments show 90% probability regions for the population implied by individual hyper-parameter draws. The mean of these regions is outlined in black.

can be easily interpreted via a single parameter. Equally appealing is their ease of use, effectively acting as modular additions to existing models.

ACKNOWLEDGEMENTS

We thank Tom Callister, Maya Fishbach, and our anonymous referee for insightful comments and discussion of the work presented here. We also thank Shanika Galaudage for her assistance in utilising the `GWPopulation` package. We acknowledge support from the Australian Research Council (ARC) Centre of Excellence CE170100004. This material is based upon work supported by NSF’s LIGO Laboratory which is a major facility fully funded by the National Science Foundation. The authors are grateful for computational resources provided by the LIGO Laboratory and supported by National Science Foundation Grants PHY-0757058 and PHY-0823459. This re-

search has made use of data or software obtained from the Gravitational Wave Open Science Center (gw-openscience.org), a service of LIGO Laboratory, the LIGO Scientific Collaboration, the Virgo Collaboration, and KAGRA. LIGO Laboratory and Advanced LIGO are funded by the United States National Science Foundation (NSF) as well as the Science and Technology Facilities Council (STFC) of the United Kingdom, the Max-Planck-Society (MPS), and the State of Niedersachsen/Germany for support of the construction of Advanced LIGO and construction and operation of the GEO600 detector. Additional support for Advanced LIGO was provided by the Australian Research Council. Virgo is funded, through the European Gravitational Observatory (EGO), by the French Centre National de Recherche Scientifique (CNRS), the Italian Istituto Nazionale di Fisica Nucleare (INFN) and the Dutch Nikhef, with contributions by institutions from Belgium, Germany, Greece, Hungary, Ireland, Japan, Monaco, Poland, Portugal, Spain. The construction and operation of KAGRA are funded by Ministry of Education, Culture,

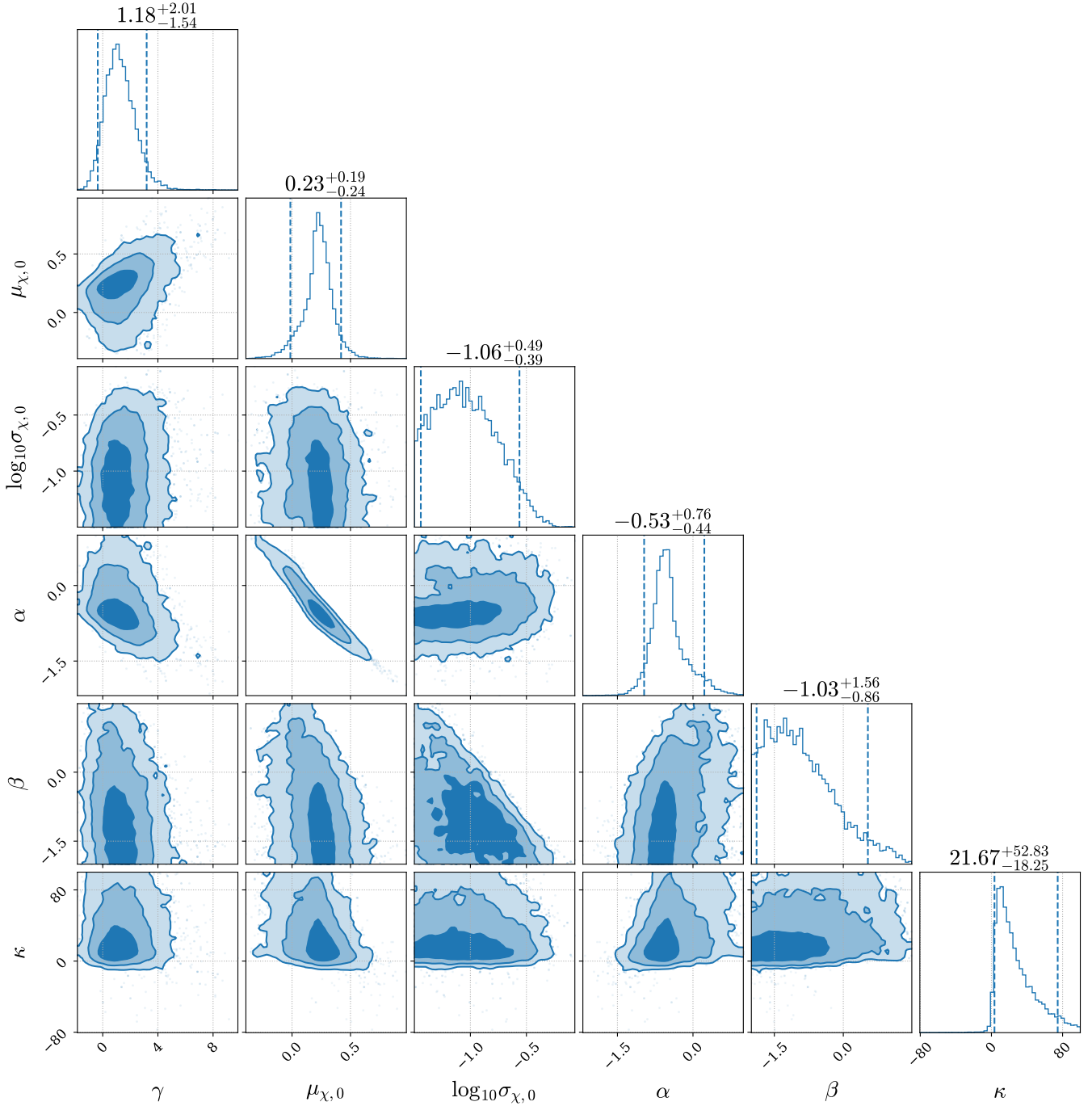


Figure 5. Corner plot of the posteriors for hyper-parameters governing the distribution of mass ratio and effective inspiral spin. Contours on the two-dimensional plots, from darkest to lightest, show 50, 90 and 99%-credible regions, whilst blue dashed lines on one-dimensional plots show 90%-credible regions. Values listed above give the median of the posterior as well as the aforementioned 90%-credible region.

Sports, Science and Technology (MEXT), and Japan Society for the Promotion of Science (JSPS), National Research Foundation (NRF) and Ministry of Science and ICT (MSIT) in Korea, Academia Sinica (AS) and the Ministry of Science and Technology (MoST) in Taiwan.

DATA AVAILABILITY

We analyse data from [Abbott et al. \(2021b\)](#), made publicly available through [Abbott et al. \(2021c\)](#). This work also presents results from [Callister et al. \(2021\)](#). The modified version of GWPopulation used in this analysis is publicly available at https://github.com/ChristianAdamcewicz/gwpopulation/tree/q_chi_eff_cal_copula.

REFERENCES

- Aas K., Czado C., Frigessi A., Bakken H., 2009, *Insurance: Math. and Economics*, 44, 182
- Aasi J., et al., 2015, *Class. Quantum Grav.*, 32, 074001
- Abbott R., et al., 2019, *ApJ*, 882, L24
- Abbott R., et al., 2021a, The population of merging compact binaries inferred using gravitational waves through GWTC-3 ([arXiv:2111.03634](#))
- Abbott R., et al., 2021b, *Phys. Rev. X*, 11, 021053
- Abbott R., et al., 2021c, *SoftwareX*, 13, 100658
- Abbott R., et al., 2021d, *ApJ*, 913, L7
- Acernese F., et al., 2015, *Class. Quantum Grav.*, 32, 024001
- Andreani P., et al., 2014, *A&A*, 566, A70
- Andreani P., Boselli A., Ciesla L., Vio R., Cortese L., Buat V., Miyamoto Y., 2018, *A&A*, 617, A33
- Ashton G., et al., 2019, *ApJS*, 241, 27
- Baibhav V., Gerosa D., Berti E., Wong K. W. K., Helfer T., Mould M., 2020, *Phys. Rev. D*, 102, 043002
- Bavera S. S., et al., 2020, *A&A*, 635, A97
- Bavera S. S., et al., 2021, *A&A*, 647, A153
- Bavera S. S., Fishbach M., Zevin M., Zapartas E., Fragos T., 2022, The χ_{eff} - z correlation of field binary black hole mergers and how 3G gravitational-wave detectors can constrain it ([arXiv:2204.02619](#))
- Bedford T., Cooke R. M., 2002, *Ann. Statist.*, 30, 1031
- Belczynski K., Holz D. E., Bulik T., O'Shaughnessy R., 2016a, *Nature*, 534, 512
- Belczynski K., et al., 2016b, *A&A*, 594, A97
- Belczynski K., Doctor Z., Zevin M., Olejak A., Banerjee S., Chattopadhyay D., 2022, Black hole - black hole total merger mass and the origin of LIGO/Virgo sources ([arXiv:2204.11730](#))
- Biscoveanu S., Callister T. A., Haster C.-J., Ng K. K. Y., Vitale S., Farr W. M., 2022, *ApJ*, 932, L19
- Blyth C. R., 1972, *Journal of the American Statistical Association*, 67, 364
- Bogdanović T., Reynolds C. S., Miller M. C., 2007, *ApJ*, 661, L147
- Bouffanais Y., Mapelli M., Santoliquido F., Giacobbo N., Carlo U. N. D., Rastello S., Artale M. C., Iorio G., 2021, *MNRAS*, 507, 5224
- Bouyé E., Durrleman V., Nikeghbali A., Riboulet G., Roncalli T., 2000, *SSRN*
- Broekgaarden F. S., Stevenson F., Thrane E., 2022, Signatures of mass ratio reversal in gravitational waves from merging binary black holes ([arXiv:2205.01693](#))
- Callister T. A., 2021, A Thesaurus for Common Priors in Gravitational-Wave Astronomy ([arXiv:2104.09508](#))
- Callister T. A., Haster C.-J., Ng K. K. Y., Vitale S., Farr W. M., 2021, *ApJ*, 922, L5
- Callister T. A., Miller S. J., Chatziioannou K., Farr W. M., 2022, No evidence that the majority of black holes in binaries have zero spin ([arXiv:2205.08574](#))
- Damour T., 2001, *Phys. Rev. D*, 64, 124013
- Devroye L., Letac G., 2010, Copulas in three dimensions with prescribed correlations ([arXiv:1004.3146](#))
- Doctor Z., Wysocki D., O'Shaughnessy R., Holz D. E., Farr B., 2020, *ApJ*, 893, 35
- Farr B., Holz D. E., Farr W. M., 2018, *ApJ*, 854, L9
- Fishbach M., Holz D. E., Farr B., 2017, *ApJ*, 840, L24
- Fishbach M., et al., 2021, *ApJ*, 912, 98
- Franciolini G., Pani P., 2022, *Phys. Rev. D*, 105, 123024
- Galaudage S., Talbot C., Nagar T., Jain D., Thrane E., Mandel I., 2021, *ApJ*, 921, L15
- Gerosa D., Berti E., 2017, *Phys. Rev. D*, 95, 124046
- Gondán L., Kocsis B., 2021, *MNRAS*, 506, 1665
- Gunawardhana M. L. P., et al., 2014, *MNRAS*, 447, 875
- Hinder I., Vaishnav B., Herrmann F., Shoemaker D. M., Laguna P., 2008, *Phys. Rev. D*, 77, 081502(R)
- Hoy C., Fairhurst S., Hannam M., Tiwari V., 2022, *ApJ*, 928, 75
- Jiang I.-G., Yeh L.-C., Chang Y.-C., Hung W.-L., 2008, *AJ*, 137, 329
- Kimball C., Talbot C., Berry C. P. L., Carney M., Zevin M., Thrane E., Kalogera V., 2020, *ApJ*, 900, 177
- Kimball C., Talbot C., Berry C. P., Zevin M., Thrane E., et al., 2021, *ApJ*, 915, L35
- Kruckow M. U., Han Z., 2021, Unexpected correlations in outstanding subpopulations of the gravitational wave transient catalogue data ([arXiv:2112.07847](#))
- Lin C.-A., Kilbinger M., 2015, *A&A*, 576, A24
- Lousto C. O., Nakano H., Zlochower Y., Campanelli M., 2010, *Phys. Rev. D*, 81, 084023
- Lower M. E., Thrane E., Lasky P. D., Smith R., 2018, *Phys. Rev. D*, 98, 083028
- Mandel I., Farmer A., 2022, *Phys. Reports*, 955, 1
- Mandel I., de Mink S. E., 2016, *MNRAS*, 458, 2634
- Mapelli M., 2018, Astrophysics of stellar black holes ([arXiv:1809.09130](#))
- Mapelli M., Bouffanais Y., Santoliquido F., Arca-Sedda M., Artale M. C., 2022, *MNRAS*, 511, 5797
- Marchant P., Langer N., Podsiadlowski P., Tauris T. M., Moriya T. J., 2016, *A&A*, 588, A50
- Marchant P., Renzo M., Farmer R., Pappas K. M. W., Taam R. E., de Mink S. E., Kalogera V., 2019, *ApJ*, 882, 36
- McKernan B., Ford K. E. S., Callister T., Farr W. M., O'Shaughnessy R., Smith R., Thrane E., Vajpeyi A., 2022, *MNRAS*, 514, 3886
- Mould M., Gerosa D., Broekgaarden F. S., Steinle N., 2022, Which black hole merger first? Mass-ratio reversal in massive binary stars from gravitational-wave data ([arXiv:2205.12329](#))
- Neijssel C. J., et al., 2019, *MNRAS*, 490, 3740
- O'Leary R. M., Meiron Y., Kocsis B., 2016, *ApJ*, 824, L12
- Peters P. C., 1964, *Phys. Rev.*, 136, B1224
- Qin Y., Fragos T., Meynet G., Andrews J., Sørensen M., Song H. F., 2018, *A&A*, 616, A28
- Qin J., Yu Y., Zhang P., 2020, *ApJ*, 897, 105
- Rodriguez C. L., Morscher M., Pattabiraman B., Chatterjee S., Haster C.-J., Rasio F. A., 2015, *Phys. Rev. Lett.*, 115, 051101
- Rodriguez C. L., Zevin M., Pankow C., Kalogera V., Rasio F. A., 2016, *ApJ*, 832, L2
- Rodriguez C. L., Amaro-Seoane P., Chatterjee S., Kremer K., Rasio F. A., Samsing J., Ye C. S., Zevin M., 2018, *Phys. Rev. D*, 98, 123005
- Romero-Shaw I. M., Lasky P. D., Thrane E., 2019, *MNRAS*, 490, 5210
- Romero-Shaw I. M., Talbot C., Biscoveanu S., et al., 2020, *MNRAS*, 499, 3295
- Roulet J., Chia H. S., Olsen S., Dai L., Venumadhav T., Zackay B., Zaldarriaga M., 2021, *Phys. Rev. D*, 104, 083010
- Safarzadeh M., Farr W. M., Ramirez-Ruiz E., 2020, *ApJ*, 894, 129
- Samsing J., 2018, *Phys. Rev. D*, 97, 103014
- Samsing J., Ramirez-Ruiz E., 2017, *ApJ*, 840, L14
- Samsing J., MacLeod M., Ramirez-Ruiz E., 2014, *ApJ*, 784, 71
- Sato M., Ichiki K., Takeuchi T. T., 2010, *Phys. Rev. Lett.*, 105
- Scherrer R. J., Berlind A. A., Mao Q., McBride C. K., 2009, *ApJ*, 708, L9
- Schnittman J. D., 2004, *Phys. Rev. D*, 70, 124020
- Sklar A., 1996, *Lecture Notes-Monograph Series*, 28, 1
- Speagle J. S., 2020, *MNRAS*, 493, 3132
- Spera M., Trani A. A., Mencagli M., 2022, *Galaxies*, 10, 76
- Stevenson S., Vigna-Gómez A., Mandel I., Barrett J. W., Neijssel C. J., Perkins D., de Mink S. E., 2017, *Nature Communications*, 8, 14906
- Stevenson S., Sampson M., Powell J., Vigna-Gómez A., Neijssel C. J., Szécsi D., Mandel I., 2019, *ApJ*, 882, 121
- Stone N. C., Metzger B. D., Haiman Z., 2016, *MNRAS*, 464, 946
- Takeuchi T. T., 2010, *MNRAS*, 406, 1830
- Takeuchi T. T., Kono K. T., 2020, *MNRAS*, 498, 4365
- Takeuchi T. T., Sakurai A., Yuan F.-T., Buat V., Burgarella D., 2013, *Earth, Planets and Space*, 65, 281
- Talbot C., Thrane E., 2017, *Phys. Rev. D*, 96, 023012
- Talbot C., Thrane E., 2018, *ApJ*, 856, 173
- Talbot C., Smith R., Thrane E., Poole G. B., 2019, *Phys. Rev. D*, 100, 043030
- Thrane E., Talbot C., 2019, *Publ. Astron. Soc. Australia*, 36, e010
- Tiwari V., 2022, *ApJ*, 928, 155
- Vajpeyi A., Thrane E., Smith R., McKernan B., Ford K. S., 2022, *ApJ*, 931, 82
- Wong K. W. K., Breivik K., Kremer K., Callister T., 2021, *Phys. Rev. D*, 103, 083021

- Woosley S. E., Heger A., 2021, *ApJ*, 912, L31
 Wysocki D., Lange J., O’Shaughnessy R., 2019, *Phys. Rev. D*, 100, 043012
 Yu H., Ma S., Giesler M., Chen Y., 2020, *Phys. Rev. D*, 102, 123009
 Yuan Z., Wang J., Worrall D. M., Zhang B.-B., Mao J., 2018, *ApJS*, 239, 33
 Zevin M., Bavera S. S., 2022, *ApJ*, 933, 86
 Zevin M., Samsing J., Rodriguez C., Haster C.-J., Ramirez-Ruiz E., 2019, *ApJ*, 871, 91
 Zevin M., et al., 2021, *ApJ*, 910, 152
 van Son L. A. C., et al., 2022, *ApJ*, 931, 17

APPENDIX A: IMPLIED CORRELATIONS FROM COMPONENT SPIN MODELS

It is not uncommon to model the distributions of binary black hole component spin magnitudes $\chi_{1,2}$ and tilts $t_{1,2}$ instead of the χ_{eff} distribution (see, for example [Abbott et al. 2021d,a](#); [Talbot & Thrane 2017](#); [Wysocki et al. 2019](#); [Galaudage et al. 2021](#)). Given that the definition of χ_{eff} depends on the mass ratio q (see equation 2), one might wonder if models described in terms of independently distributed physical parameters,

$$\pi(q, \chi_1, \chi_2, \dots) = \pi(q)\pi(\chi_1)\pi(\chi_2)\dots \quad (\text{A1})$$

imply (inadvertent) correlation between (q, χ_{eff}) . We explore this possibility using the DEFAULT model described in [Abbott et al. \(2021a\)](#) (see also [Talbot & Thrane 2017](#); [Wysocki et al. 2019](#)). Using distributions reconstructed with the best-fit hyper-parameters, we draw 2.5×10^4 samples for $(q, \chi_1, \chi_2, \cos t_1, \cos t_2)$, and then convert these to χ_{eff} samples using equation 2.

We then measure the correlation between q and χ_{eff} in these samples. To do so, we make use of the known marginal distribution for q , and a suitable approximation of the marginal distribution for χ_{eff} obtained using a Gaussian kernel density estimate. We then construct a simple model for the joint distribution of (q, χ_{eff}) by linking the known marginal distributions with a Frank copula density function dependent on a correlation parameter κ_{default} (see Section 3 for details). This allows us to perform a simple one-dimensional fit for κ_{default} – the correlation in the $q - \chi_{\text{eff}}$ plane implied by the DEFAULT model. The results of this analysis are shown in Fig. A1.

We find that the DEFAULT model does not imply a strong correlation between q and χ_{eff} . This suggests that the (q, χ_{eff}) correlation observed by [Callister et al. \(2021\)](#), and discussed in Section 5, is not a predetermined consequence of the parameterisation of χ_{eff} .

This paper has been typeset from a \LaTeX file prepared by the author.

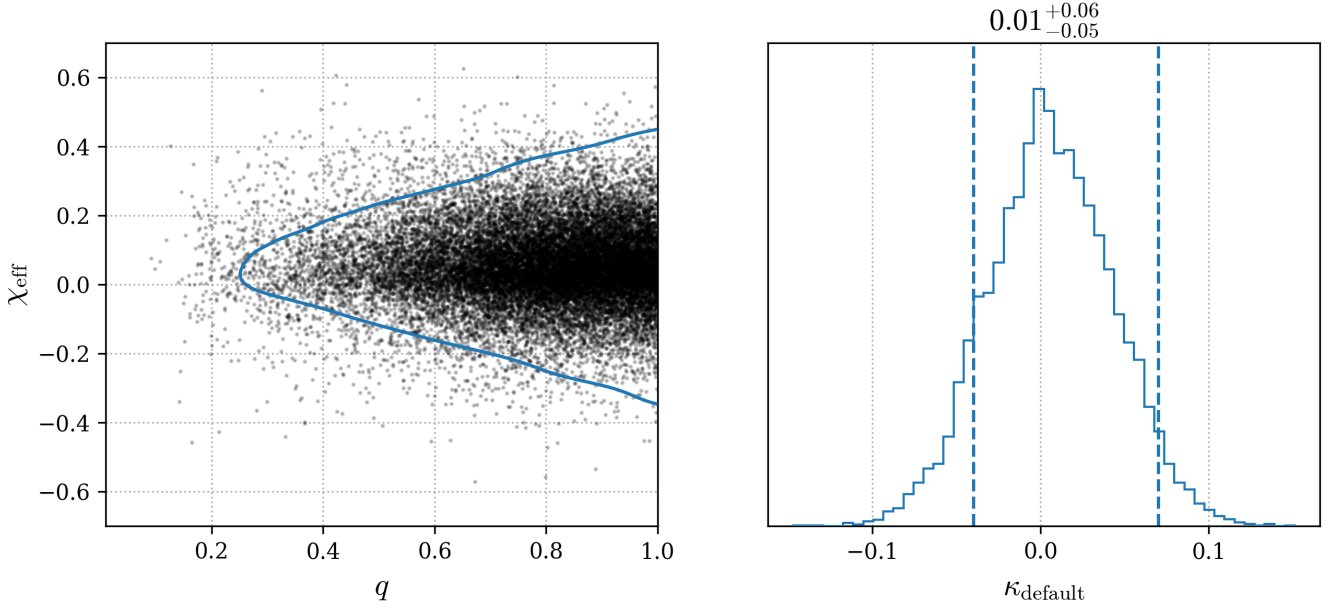


Figure A1. Correlation between mass ratio and effective inspiral spin implied by the independently distributed component spins of the DEFAULT model. **Left:** joint distribution of mass ratio and effective inspiral spin implied by the DEFAULT model. Samples generated using the model are shown in black. The blue line shows the reconstructed distribution using the best-fit value for the correlation parameter κ_{default} . **Right:** posterior distribution for κ_{default} . The blue dashed lines show the 90% credible regions. These along with the median of the posterior distribution are listed above.